PCCP

Accepted Manuscript

ROYAL SOCIETY OF CHEMISTRY

www.rsc.org/pccp

Journal Name

RSCPublishing

COMMUNICATION

Cite this: DOI: 10.1039/x0xx00000x

Hierarchical Ni-Co-O@Ni-Co-S Nanoarray as Advanced Oxygen Evolution Reaction Electrode

Received 00th January 2012,
Accepted 00th January 2012

DOI: 10.1039/x0xx00000x

www.rsc.org/

Wenwen Xu[a], Zhiyi Lu[a], Xiaodong Lei[a], Yaping Li[a], and Xiaoming Sun*[a]

Developing an efficient electro-catalyst for water oxidation is essential for improving the performance, which holds the key for a number of energy conversion and storage devices. Here we report an effective method for fabricating a Ni-Co-O@Ni-Co-S hierarchical nanoarray, which showed a significantly improved activity relative to Ni-Co-O nanowire arrays for oxygen evolution reaction. The enhanced performance was attributed to the secondary formed Ni-Co-S nanoplatelets which not only acted as an efficient electrocatalyst, but also facilitated the electrolyte penetration and increased the surface area.

The fast consumption of fossil fuels caused by industrial and transportation activities accelerates the demand of clean energy (e.g. hydrogen production) and energy storage devices (e.g. metal air batteries).[1-5] The keys of two of the above energy systems (water splitting and zinc-air battery) are held by the electrochemical water oxidation reaction, which involves a 4-electron transfer process to form one molecular oxygen.[6, 7] However, the sluggish kinetic of the oxygen evolution reaction (OER) is the major limitation for achieving higher performance[8], which motivates the researchers to keep identifying more active catalysts.[9-11] Although precious metal oxides (e.g. RuO_2 and IrO_2)[12, 13] are currently the best catalysts for OER, the scarcity and high cost greatly restrict their large-scale applications. Instead, cobalt and nickel based compounds, including phosphate[6], perovskites[14], borate[15, 16], and oxides[17-22], have been widely investigated as alternative candidates due to the relatively low cost and desirable performance. However, the issues of relatively poor conductivity and limited active sites exposure of the catalysts should be addressed to improve the catalytic performance.

Constructing an ideal structure for the catalysts is an efficient approach to meet the aforementioned problems. Previous researches have demonstrated that vertically aligned nanoarray architecture can offer a number of benefits, thereby bringing about a dramatic improvement in the electrochemical performance of the active material over slurry-cast electrodes for gas evolution reaction.[23, 24] Specifically, this kind of architecture provides a tight contact to the current collector, a direct electron pathway and a high porosity, thus facilitating electron transportation, accelerating electrolyte penetration and increasing the electrochemically active surface area.[25, 26] Moreover, the nanoarray architecture significantly reduces the releasing size of as-formed gas bubbles, thus offering a stable and fast current increase.[27] Hierarchical nanoarray architecture, which provides an even higher porosity and more abundant active sites[28, 29], should be more desirable for electrochemical catalysis.

Herein, a hierarchical Ni-Co-O@Ni-Co-S nanoarray (Ni-Co-O@Ni-Co-S NA) where small Ni-Co-S nanoplatelets were grown outside of Ni-Co-O nanowires backbone on conductive substrates was fabricated by a three-step process, which involved a hydrothermal reaction, room-temperature transformation and subsequent calcination. As an integrated electrode for OER, this hierarchical nanoarray exhibited a high activity with an onset potential of ~1.51 V vs. reversible hydrogen electrode (RHE) and a fast current increase, thus achieving a high current density (~20 mA cm^{-2}) with a small overpotential of ~300 mV (η_{20}), much better than pure Ni-Co-O nanowire array (Ni-Co-O NWA). The enhancement in the OER performance was attributed to the unique hierarchical architecture and the introduction of secondary Ni-Co-S nanoplatelets. In addition, this hierarchical nanoarray showed a prominent stability at a high reaction rate for a long time. This work not only discovered a new and efficient OER catalyst (Ni-Co-S), but also provided a new opportunity for constructing advanced structures for next generation water splitting and metal-air battery devices.

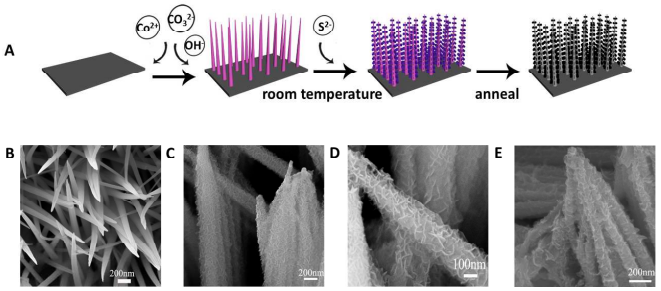

Figure 1. (A), Schematic illustration of the synthesis of hierarchical Ni-Co-O@Ni-Co-S nanoarray; (B), Typical SEM image of Ni-doped $Co_2(OH)_2CO_3$ nanowires array; (C) and (D), SEM images of the Ni-

doped $Co_2(OH)_2CO_3$@CoS hierarchical nanoarray with different magnifications; (E), SEM image of the final product after annealing.

The synthesis process of the hierarchical Ni-Co-O@Ni-Co-S NA was schematically shown in Figure 1A. The nickel foam was chosen here as the substrate because of its zig-zag skeleton and high porosity, which helped to increase the active surface area.[30] Nickel doped cobalt hydroxide carbonate nanowires array was firstly grown on nickel foam by a simple hydrothermal reaction. The doping of Ni was caused by the dissolution and precipitation of the nickel foam substrate (detailed discussion can be seen in supporting information). Afterwards, Ni-Co-S nanoplatelets were *in-situ* formed along the nanowire backbone by simply immersing in 1 M Na_2S solution at room temperature overnight. Finally, the precursor was converted to hierarchical Ni-Co-O@Ni-Co-S NA by a calcination process. The morphology of the as-synthesized Ni-Co-O@Ni-Co-S NA was examined with scanning electron microscopy (SEM). The pristine NWA showed a smooth surface of each nanowire (Fig. 1B) while a large quantity of small platelets formed outside of the nanowires was observed after room-temperature transformation (Fig. 1C). The average size of the secondary grown nanoplatelets was about 50 nm, which would brought about a much higher roughness of the nanoarray (Fig. 1D). The subsequent calcination did not destroy the surface morphology (Fig. 1E) and well preserved the hierarchical porosity, which was confirmed by the TEM image (Fig. S1). Moreover, the energy dispersive spectroscopy results (EDS, Fig. S2) demonstrated the uniform distribution of metal throughout the hierarchical structure and the existence of S at the outside. The Ni/Co ratios of the nanowires and hierarchical structures were both 1:4 (Table S1).

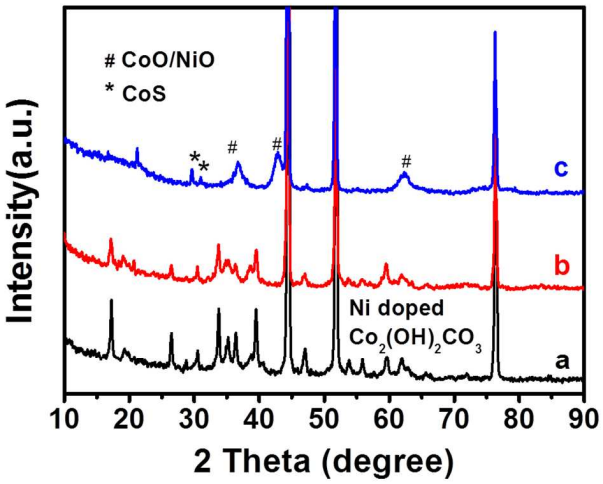

Figure 2. XRD patterns of as-synthesized three samples. (a: Ni-doped $Co(OH)_2CO_3$; b: the sample after room temperature transformation at 1 M Na_2S solution; c: hierarchical Ni-Co-O@Ni-Co-S nanoarray)

This *in situ* morphology evolution process can indeed lead to a phase transformation.[31] Fig. 2 showed the X-ray diffraction (XRD) patterns of the three samples. The phase of the original NWAs can be indexed to the $Co_2(OH)_2CO_3$ phase (line a, JCPDF: 48-0083). After the room-temperature transformation, the intensity of original peaks was weaker and no other peak was shown (line b), indicating that the nanowires became thinner and the secondary formed nanoplatelets were amorphous. The blue line (line c) demonstrated that hydroxide carbonates were converted to oxides (JCPDF: 65-2902; 44-1159) after calcination process, which also crystallized the layered hexagonal Ni-Co-S nanoplatelets. The peaks marked "#" were indexed to CoS (JCPDF: 65-8977) and the peak located at $2\theta \approx 21°$ may be index to $Ni_{3-x}S_2$ (JCPDF: 14-0358). The X-ray photoelectron spectroscopy results (XPS, Fig. S3) further confirmed the formation of CoS with Co $2p_{3/2}$ and S $2p_{3/2}$ binding energy of ~781.6 eV and ~162.0 eV, respectively.[32]

On the basis of the above results, the conversion from nanowires array to hierarchical nanoarray in Na_2S solution follows an ion-exchange reaction (eq. 1);

$$Ni_xCo_{2-x}(OH)_2CO_3 + 2S^{2-} \leftrightarrow Ni_xCo_{2-x}S + 2OH^- + CO_3^{2-} \quad \text{(eq. 1)}$$

According to thermodynamic theory, nickel and cobalt hydroxide carbonate have K_{sp} values in the range of 10^{-13} and 10^{-15} (K_{sp} ($Co(OH)_2$) = 1.1×10^{-15}, K_{sp} ($Ni(OH)_2$) = 2.0×10^{-15}, K_{sp} ($CoCO_3$) = 1.4×10^{-13}), which are much higher than the K_{sp} value of nickel and cobalt sulfide (K_{sp} (CoS) = 4×10^{-21}, K_{sp} (NiS) = 1.1×10^{-21}). Thus, Ni-doped $Co_2(OH)_2CO_3$ would readily be converted to Ni-Co-S in the presence of S^{2-}, driven by the chemical potential variation. Eventually, the hierarchical and highly porous structure was obtained based on the precursive NWA.

Such a hierarchical porous film would promote electrochemical reactions on the electrode surface in virtue of the enlarged surface area and abundant active sites. Here we evaluated the OER activity of the hierarchical Ni-Co-O@Ni-Co-S NA using a typical three-electrode setup in O_2-saturated 0.1 M KOH electrolyte. The Ni-Co-O NWA was also tested as a control sample. Representative cyclic voltammetry curves (Fig. S4) revealed that the Ni-Co-O NWA exhibited two primary characteristics: a pair of redox peaks which was attributed to the Ni^{2+}/Ni^{3+} and Co^{2+}/Co^{3+} transformations was observed; and a positive (oxidation) current at potentials greater than 0.6 V vs. SCE, which was ascribed to OER. As to the Ni-Co-O@Ni-Co-S sample, the redox peaks located at similar positions to the Ni-Co-O NWA, indicating similar redox reactions occurred at this potential range[33]. However, the unclarity of the peaks was caused by the larger background current. It was found that the hierarchical Ni-Co-O@Ni-Co-S NA exhibited an onset potential (Fig. 3A, defined as the start point in the linear range of Tafel slope) of ~1.51 V vs. RHE and an overpotential of ~300 mV at ~20 mA cm^{-2} (η_{20}), which were both much lower than that of Ni-Co-O NWA (an onset potential of ~1.54 V and η_{20} of ~350 mV) and the nickel foam substrate. To gain more insight into the OER activity, Tafel plots derived from polarization curves were constructed (Fig. 3B). The resulting Tafel slope of Ni-Co-O@Ni-Co-S NA was ~89 mV dec^{-1}, which was comparable with Ni-Co-O NWA (~90 mV dec^{-1}), indicating both electrodes followed the same OER mechanism.

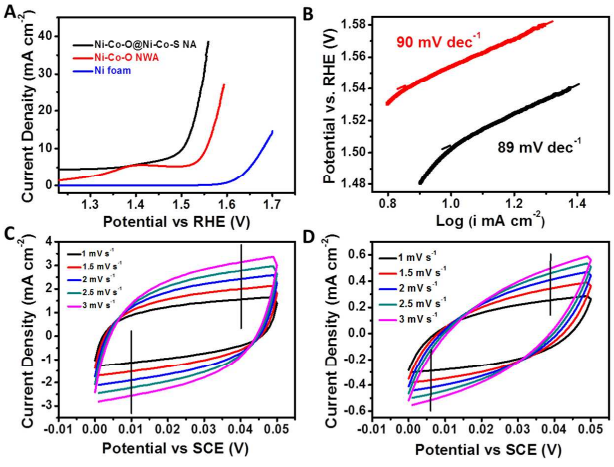

Figure 3. (A), polarization curves of hierarchical Ni-Co-O@Ni-Co-S NA, Ni-Co-O NWA and nickel foam; (B), Tafel plots of samples (black line: Ni-Co-O@Ni-Co-S NWA; red line: Ni-Co-O NA); (C) and (D), electrochemical surface area (ESA) measurements of hierarchical Ni-Co-O@Ni-Co-S NA and Ni-Co-O NWA, the crossover points by the CV curve and vertical black line are used to determine the ESA values.

The electrochemical surface area (ESA) should play an important role for the high electro-catalytic performance.[34, 35] To qualitatively evaluate the ESA values of both electrodes, we measured the non-faradic capacitive current associated with electrochemical double layer charging upon repeated potential cycling, as shown in Figure 3C and D. The double layer charging current is proportional to both the scan rate and the ESA of the electrode.[36] The potential range selected here (1.0-1.05 V vs. RHE) for the capacitance measurements did not include obvious electrochemical features corresponding to faradic current.[37] As a result, the dependence of the current on the scan rate in this region for both electrodes was linear, which was consistent with capacitive charging behavior. The capacitance of the hierarchical Ni-Co-O@Ni-Co-S NA was measured as 851.1 mF cm^{-2} (Fig. S5), corresponding to a roughness factor of 14185 assuming the capacitance of flat film was ~60 μF cm^{-2}.[37] On the contrary, the Ni-Co-O NWA only showed a much smaller double layer capacitance (141.8 mF cm^{-2}, corresponding to a roughness factor of 2363), thus demonstrating the advantage of hierarchical structure design.

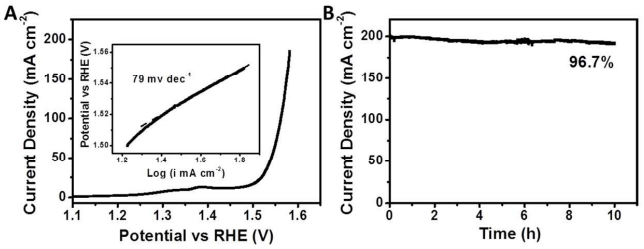

Figure 4. (A), polarization curve of the hierarchical Ni-Co-O@Ni-Co-S NA in 1 M KOH solution, the inset is the corresponding Tafel plot; (B), stability result of the hierarchical Ni-Co-O@Ni-Co-S NA at a high current density, the applied potential is 1.6 V after IR-correction.

The current density was hardly to reach hundreds of milliamperes per square centimeter (refer to the geometric area) which was required for industrial application, due to the limited OH^- concentration in an electrolyte with a pH value of ~13. Therefore, we measured the OER activity of the hierarchical Ni-Co-O@Ni-Co-S NA in 1 M KOH solution, and as expected, this hierarchical electrode was more active with a lower Tafel slope (~79 mV dec^{-1}) and a much higher current density (~100 mA cm^{-2}) at a potential of 1.56 V, as shown in Figure 4A. Moreover, the hierarchical Ni-Co-O@Ni-Co-S NA showed a high and stable current density (~200 mA cm^{-2}) with negligible degradation for 10 h when operating OER at a constant overpotential, indicating a prominent stability. Combination of the above features (small overpotential and high durability) validates the hierarchical Ni-Co-O@Ni-Co-S NA as an advanced and promising OER electrode.

Obviously, the significantly enhanced OER performance is attributed to the secondary formed Ni-Co-S nanoplatelets, which lead to the formation of a hierarchical structure. Ni and Co are generally considered as the active center for OER because of its suitable binding energy (not too strong not too weak) to oxygen intermediates.[8, 38] Moreover, it is found that coordination of other anions can affect the electronic structure, which further improves the corresponding OER activity.[16, 39-41] Indeed, transition metal chalcogenides have been investigated with ultrahigh OER activities.[30, 42] Therefore, it is reasonable that Ni-Co-S is a potential electro-catalyst for water oxidation.

More importantly, the unique hierarchical architecture should play an essential role in enhancing the OER activity. Compared with the nanowire array, the hierarchical nanoarray can offer an even higher surface area and porosity, while the conductivity can be well preserved. The ESA results (Fig. 3C and D) clearly demonstrated the higher surface area of the hierarchical architecture, which resulted in a higher active sites density in a certain geometric area. In addition, the hierarchical porosity could accelerate the diffusion of the OH^- ions, thus resulting in faster kinetics. Therefore, the improved OER performance of the hierarchical Ni-Co-O@Ni-Co-S NA could be easily understood by a combination of inducing a more active electro-catalyst and constructing a hierarchical architecture at the electrode surface.

In summary, a facile and cost-effective method was developed to construct a hierarchical Ni-Co-O@Ni-Co-S nanoarray on Ni foam, which exhibited superior OER activity to the Ni-Co-O nanowire array. The advanced architecture design and the presence of active catalyst (Ni-Co-S) could be the main reason for the enhanced performance. Combination of the outstanding OER features (a small overpotential, good stability and large anodic current density) endows the hierarchical Ni-Co-O@Ni-Co-S nanoarray as a new and promising active electrode for the next generation oxygen-related devices.

This work was supported by National Natural Science Foundation of China, the 973 Program (2011 CBA00503 and 2011CB932403), an the Program for New Century Excellent Talents in Universities, the Program for Changjiang Scholars and Innovative Research Team in University.

Notes and references

[a] *State Key Laboratory of Chemical Resource Engineering, Beijing University of Chemical Technology, Beijing 100029, China*
Tel.: +86-10-64448751. Fax: +86-10-64425385.
E-mail: sunxm@mail.buct.edu.cn

Electronic Supplementary Information (ESI) available: [experimental section, XPS survey, mapping data, electrochemical surface area results]. See DOI: 10.1039/c000000x/

1. M. G. Walter, E. L. Warren, J. R. McKone, S. W. Boettcher, Q. Mi, E. A. Santori and N. S. Lewis, *Chem. Rev.*, 2010, **110**, 6446-6473.
2. T. R. Cook, D. K. Dogutan, S. Y. Reece, Y. Surendranath, T. S. Teets and D. G. Nocera, *Chem. Rev.*, 2010, **110**, 6474-6502.
3. A. I. Hochbaum and P. Yang, *Chem. Rev.*, 2009, **110**, 527-546.
4. Z.-L. Wang, D. Xu, J.-J. Xu and X.-B. Zhang, *Chem. Soc. Rev.*, 2014, **DOI: 10.1039/C3CS60248F**.
5. Y. Li, M. Gong, Y. Liang, J. Feng, J.-E. Kim, H. Wang, G. Hong, B. Zhang and H. Dai, *Nat. Commun.*, 2013, **4**, 1805-1811.
6. M. W. Kanan and D. G. Nocera, *Science*, 2008, **321**, 1072-1075.

7. J. Wang, H. x. Zhong, Y. l. Qin and X. b. Zhang, *Angew. Chem. Int. Ed.*, 2013, **125**, 5356-5361.
8. I. C. Man, H. Y. Su, F. Calle‐Vallejo, H. A. Hansen, J. I. Martínez, N. G. Inoglu, J. Kitchin, T. F. Jaramillo, J. K. Nørskov and J. Rossmeisl, *Chem. Cat. Chem*, 2011, **3**, 1159-1165.
9. M. Gong, Y. Li, H. Wang, Y. Liang, J. Z. Wu, J. Zhou, J. Wang, T. Regier, F. Wei and H. Dai, *J. Am. Chem. Soc.*, 2013, **135**, 8452-8455.
10. M. W. Louie and A. T. Bell, *J. Am. Chem. Soc.*, 2013, **135**, 12329-12337.
11. R. D. Smith, M. S. Prévot, R. D. Fagan, Z. Zhang, P. A. Sedach, M. K. J. Siu, S. Trudel and C. P. Berlinguette, *Science*, 2013, **340**, 60-63.
12. E. Tsuji, A. Imanishi, K.-i. Fukui and Y. Nakato, *Electrochim. Acta*, 2011, **56**, 2009-2016.
13. J.-M. Hu, J.-Q. Zhang and C.-N. Cao, *Int. J. Hydrogen. Energ.*, 2004, **29**, 791-797.
14. J. Suntivich, K. J. May, H. A. Gasteiger, J. B. Goodenough and Y. Shao-Horn, *Science*, 2011, **334**, 1383-1385.
15. D. K. Bediako, Y. Surendranath and D. G. Nocera, *J. Am. Chem. Soc.*, 2013, **135**, 3662-3674.
16. D. K. Bediako, B. Lassalle-Kaiser, Y. Surendranath, J. Yano, V. K. Yachandra and D. G. Nocera, *J. Am. Chem. Soc.*, 2012, **134**, 6801-6809.
17. B. S. Yeo and A. T. Bell, *J. Am. Chem. Soc.*, 2011, **133**, 5587-5593.
18. J. Wu, Y. Xue, X. Yan, W. Yan, Q. Cheng and Y. Xie, *Nano Res.*, 2012, **5**, 521-530.
19. H. Tüysüz, Y. J. Hwang, S. B. Khan, A. M. Asiri and P. Yang, *Nano Res.*, 2013, **6**, 47-54.
20. Y. Surendranath, D. A. Lutterman, Y. Liu and D. G. Nocera, *J. Am. Chem. Soc.*, 2012, **134**, 6326-6336.
21. M. Hamdani, R.N. Singh and P. Chartier, *Int. J. Electrochem. Sci*, 2010, **5**, 556-577.
22. R.N. Singh, D. Mishra, A.S.K. Sinha and A. Singh, *Electrochem. Comm.*, 2007, **9**, 1369-1373.
23. B. L. Ellis, P. Knauth and T. Djenizian, *Adv. Mater.*, 2014, **26**, 3368-3397.
24. J. Jiang, Y. Li, J. Liu, X. Huang, C. Yuan and X. W. D. Lou, *Adv. Mater.*, 2012, **24**, 5166-5180.
25. Z. Lu, Z. Chang, W. Zhu and X. Sun, *Chem. Commun.*, 2011, **47**, 9651-9653.
26. Y. Li, P. Hasin and Y. Wu, *Adv. Mater.*, 2010, **22**, 1926-1929.
27. Z. Lu, W. Zhu, X. Yu, H. Zhang, Y. Li, X. Sun, X. Wang, H. Wang, J. Wang and J. Luo, *Adv. Mater.*, 2014, **26**, 2683-2687.
28. Z. Lu, Q. Yang, W. Zhu, Z. Chang, J. Liu, X. Sun, D. G. Evans and X. Duan, *Nano Res.*, 2012, **5**, 369-378.
29. L. Yu, G. Zhang, C. Yuan and X. W. D. Lou, *Chem. Commun.*, 2013, **49**, 137-139.
30. W. Zhou, X.-J. Wu, X. Cao, X. Huang, C. Tan, J. Tian, H. Liu, J. Wang and H. Zhang, *Energy Environ. Sci.*, 2013, **6**, 2921-2924.
31. W. Zhu, Z. Lu, G. Zhang, X. Lei, Z. Chang, J. Liu and X. Sun, *J. Mater. Chem. A*, 2013, **1**, 8327-8331.
32. J.-Y. Lin, J.-H. Liao and S.-W. Chou, *Electrochim. Acta*, 2011, **56**, 8818-8826.
33. F. Tao, Y.-Q. Zhao, G.-Q. Zhang and H.-L. Li, *Electrochem. Comm.*, 2007, **9**, 1282-1287.
34. D. Merki, H. Vrubel, L. Rovelli, S. Fierro and X. Hu, *Chem. Sci.*, 2012, **3**, 2515-2525.
35. R. Singh, J. Pandey, N. Singh, B. Lal, P. Chartier and J.-F. Koenig, *Electrochim. Acta*, 2000, **45**, 1911-1919.
36. J. D. Benck, Z. Chen, L. Y. Kuritzky, A. J. Forman and T. F. Jaramillo, *ACS Catal.*, 2012, **2**, 1916-1923.
37. B. Lu, D. Cao, P. Wang, G. Wang and Y. Gao, *Int. J. Hydrogen. Energ.*, 2011, **36**, 72-78.
38. M. E. Lyons and M. P. Brandon, *J. Electroanal. Chem.*, 2010, **641**, 119-130.
39. S. W. Lee, C. Carlton, M. Risch, Y. Surendranath, S. Chen, S. Furutsuki, A. Yamada, D. G. Nocera and Y. Shao-Horn, *J. Am. Chem. Soc.*, 2012, **134**, 16959-16962.
40. S. Pintado, S. Goberna-Ferrón, E. C. Escudero-Adán and J. R. n. Galán-Mascarós, *J. Am. Chem. Soc.*, 2013, **135**, 13270-13273.
41. A. Grimaud, K. J. May, C. E. Carlton, Y.-L. Lee, M. Risch, W. T. Hong, J. Zhou and Y. Shao-Horn, *Nat. Commun.*, 2013, **4**, 2439-2445.
42. M.-R. Gao, Y.-F. Xu, J. Jiang, Y.-R. Zheng and S.-H. Yu, *J. Am. Chem. Soc.*, 2012, **134**, 2930-2933.